NJC

ROYAL SOCIETY OF CHEMISTRY

PAPER

View Article Online
View Journal | View Issue

Cite this: *New J. Chem.*, 2021, **45**, 8166

Design, synthesis, antibacterial activity evaluation and molecular modeling studies of new sulfonamides containing a sulfathiazole moiety†

Tuğba Meşeli,[ab] Şengül Dilem Doğan,[*b] Miyase Gözde Gündüz,[c] Zülbiye Kökbudak,[a] Sanja Skaro Bogojevic,[d] Theresa Noonan,[e] Sandra Vojnovic,[d] Gerhard Wolber[e] and Jasmina Nikodinovic-Runic[d]

Received 10th January 2021,
Accepted 25th March 2021

DOI: 10.1039/d1nj00150g

rsc.li/njc

Sulfonamides represent the oldest synthetic antibacterial agents; however, their central position in controlling bacterial diseases has been seriously damaged by the development of widespread resistance. Herein, we revisited sulfathiazole, a commercial member of antibacterial sulfa drugs, intending to overcome sulfonamide resistance and identify new drug candidates through molecular modifications. We synthesized twelve sulfonamides (**SA1–SA12**) by replacing the amino group on the phenyl ring with various substituents and introducing a thiophene ring on the core scaffold of sulfathiazole. The obtained compounds and additionally two commercial sulfonamides, sulfathiazole and sulfadiazine, were extensively screened for their antimicrobial activities. The results indicated that new sulfonamides, unlike traditional ones, were selectively effective against various *Staphylococcus aureus* strains. Introducing a bulky lipophilic substituent at the *para* position of the phenyl ring significantly increased the antibacterial activities of the compounds against *Staphylococcus aureus*. The compounds demonstrating favourable selectivity indices were further evaluated for their membrane potential perturbation and DNA interaction properties. The obtained data showed that these are not supporting mechanisms for the antibacterial activities of the modified sulfathiazole derivatives. In order to rationalize the activity of the three most active compounds, **SA7**, **SA11** and **SA12**, against *S. aureus* ATCC 25923, their binding hypotheses within the catalytic site of *Staphylococcus aureus* dihydropteroate synthase, the validated target enzyme of sulfonamides, were generated *via* molecular docking and further dissected using molecular dynamics simulations and dynamic 3D pharmacophores (dynophores).

Introduction

Bacterial infections have been a serious threat to public health over centuries causing significant morbidity and mortality worldwide.[1] Despite continuous efforts to develop and launch new antibacterial drugs, the rate and the spread of bacterial infections have never been stagnated.[2] The primary obstacle to bringing bacterial infections completely under control is the emergence of multidrug-resistant bacterial strains.[3] Therefore, the discovery of novel antibacterial agents with different scaffolds or a new mechanism of action is of utmost importance.

Sulfonamide is one of the most common functionalities in medicinal chemistry integrated into the structures of therapeutically valuable molecules.[4] In addition to being the first synthetic antibacterial agent, sulfonamides also provide a wide spectrum of biological activities such as carbonic anhydrase inhibition, insulin release induction, and anti-inflammation.[5,6]

Antibacterial sulfonamides, such as sulfathiazole, sulfadiazine, and sulfisoxazole (Fig. 1), exert their mechanism of action by interfering with the bacterial folate pathway.[7]

Dihydropteroate synthase (DHPS), one of the enzymes employed in folate biosynthesis, catalyzes the key reaction between dihydropteroate diphosphate (DHPP) and *p*-aminobenzoic acid (PABA) to form dihydropteroic acid.[8] Sulfonamides target the PABA binding site of DHPS through their similar chemical structures to PABA and inhibit the formation of dihydropteroic acid (Fig. 2). This interruption in the folate biosynthesis significantly suppresses bacterial growth and reproduction.[9]

[a] *Department of Chemistry, Faculty of Science, Erciyes University, 38039, Kayseri, Turkey*
[b] *Department of Basic Sciences, Faculty of Pharmacy, Erciyes University, 38039, Kayseri, Turkey. E-mail: dogandilem@gmail.com; Tel: +90 352 2076666-28032*
[c] *Department of Pharmaceutical Chemistry, Faculty of Pharmacy, Hacettepe University, Sıhhiye, 06100, Ankara, Turkey*
[d] *Institute of Molecular Genetics and Genetic Engineering, University of Belgrade, Vojvode Stepe 444a, 11000 Belgrade, Serbia*
[e] *Department of Pharmaceutical and Medicinal Chemistry, Institute of Pharmacy, Freie Universität Berlin, Königin-Luise-Str. 2 + 4, 14195 Berlin, Germany*

† Electronic supplementary information (ESI) available. See DOI: 10.1039/d1nj00150g

Fig. 1 Examples of antibacterial sulfa drugs.

Although sulfonamides were the first group of compounds that acted selectively on bacteria, their clinical use is highly limited nowadays. There are some important reasons for this limitation. One of them is that many other and more effective antibacterial agents were discovered after their registration in the 1930s. The second, and maybe the most important one, is the rapid drug resistance that occurred against sulfonamides. Other reasons that restrict the use of sulfonamides are the severe toxicity and the allergic side effects that are quite common among patients.[11]

Sulfathiazole is a short-acting antibacterial sulfa drug. Although its sole use has been replaced by less toxic alternatives, it is still present in commercial products in combination with other antibacterial agents, especially for the treatment of vaginal infections.[12]

Molecular modification is a frequently applied drug design strategy based on the chemical alteration of a lead compound.[13] This approach targets the improvement of pharmacological and pharmacokinetic profiles, such as increased potency, reduced toxicity, and enhanced chemical properties.[14] Molecular modification of existing chemical scaffolds stands also as a promising tool to overcome drug resistance observed in not only antibacterial[15] but also antitubercular and anticancer therapies.[16,17] Considering the gradually increasing antibacterial resistance worldwide, inexpensive sulfonamides might be reconsidered in the treatment of infectious diseases through appropriate structural modifications.

In light of these considerations, we aimed to carry out various molecular modifications on a representative sulfa drug, sulfathiazole, to overcome resistance and safety problems observed with traditional sulfonamides. To the core scaffold of sulfathiazole, we added the thiophene ring, which is one of the most common heterocycles in biologically active molecules including antibacterial agents.[18,19] With this modification, we aimed to extend the structure beyond the native substrate (PABA) binding pocket of DHPS. Additionally, we introduced diverse substituents on the phenyl ring instead of the amino group, which is one of the key moieties of classical sulfonamides (Fig. 3). To determine the effects of these modifications on the antibacterial activity, we tested the obtained compounds against different organisms.

Results and discussion

Chemistry

The synthetic route employed to produce the target sulfonamides (**SA1–SA12**) is outlined in Fig. 4. Initially, 2-acetylthiophene (**I**) was brominated with bromine in dichloromethane (DCM). The key starting compound 4-(thiophen-2-yl)thiazol-2-amine (**III**) was prepared in a high yield by the cyclization reaction of α-bromoketones (**II**) with thiourea under mild basic conditions. The combination of the amine (**III**) with different benzenesulfonyl chlorides (**IV**) in anhydrous pyridine at −5 °C afforded novel sulfonamides (**SA1–SA12**).

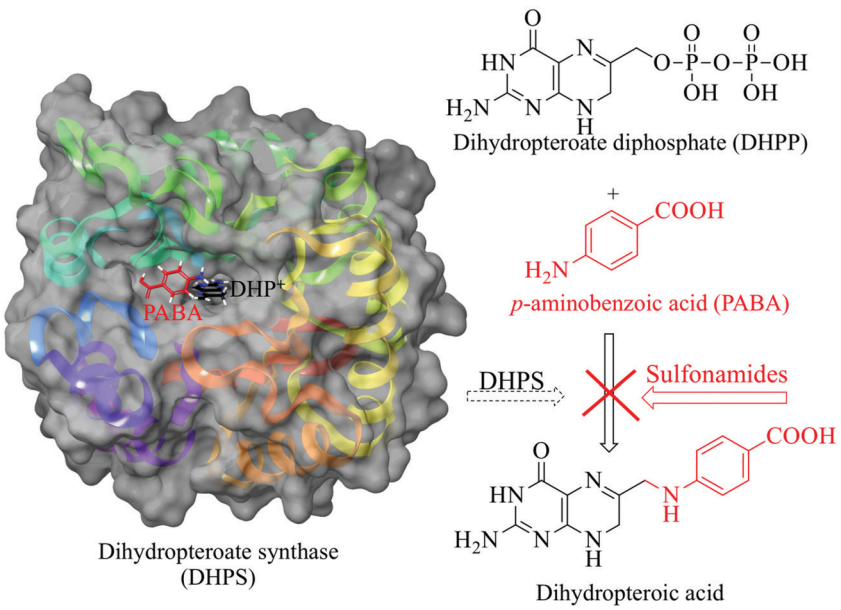

Fig. 2 Schematic representation of the antibacterial activity mechanism of sulfonamides. Molecular surface representation of DHPS with the co-crystallized PABA and DHPP (PDB code: 3TYZ)[10] represented as red and black sticks, respectively.

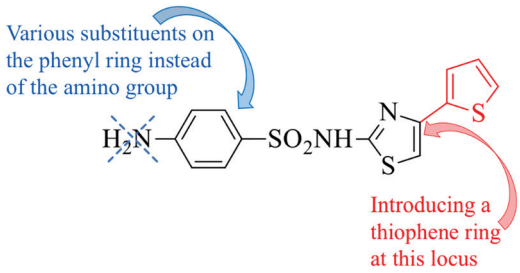

Fig. 3 Representation of the molecular modifications carried out on sulfathiazole.

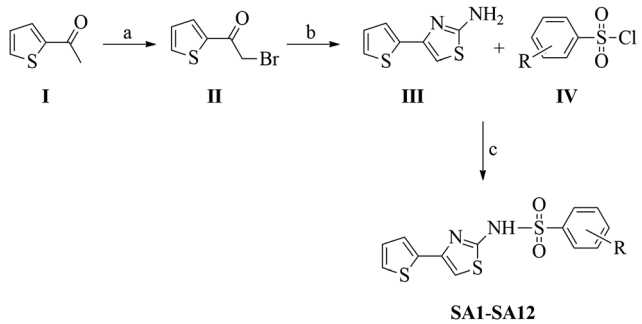

Fig. 4 Reagents and conditions: (a) bromine, DCM, 0 °C to rt, 2 h; (b) thiourea, ethanol, reflux, 2 h; (c) DCM, pyridine, −5 °C, 3 days.

In all cases, the final products (Table 1) were purified by silica gel chromatography. ^{1}H NMR, ^{13}C NMR, IR, and HRMS spectral data were used to provide a complete structural characterization of **SA1–SA12**. **SA9** was previously synthesized as an intermediate compound by Zhang *et al.*,[20] but its physicochemical properties as well as structure-elucidation data are provided for the first time in this paper.

Bioactivity assessment

Antimicrobial activity evaluation and toxicity determination. In this study, we presented the *in vitro* antimicrobial activity properties of the new sulfonamides (**SA1–SA12**) and commercial derivatives (sulfathiazole and sulfadiazine) against a wide range of bacteria (various *Staphylococcus aureus* strains, *Listeria monocytogenes*, *Pseudomonas aeruginosa*, and *Escherichia coli*) and *Candida albicans*, as a fungal representative, by determining their minimal inhibitory concentrations (MICs).

According to the obtained values, the newly synthesized sulfonamides were found to be selectively active against *Staphylococcus aureus* strains. Besides, their effects on other bacteria and fungi were lacking (activity above 200 μg mL^{-1} was not considered as a significant activity). The MIC values of **SA1–SA12** against *S. aureus* strains are reported in Table 2, and the complete data against all tested microorganisms are provided in the ESI.†

Commercial sulfonamides were not significantly effective on either bacterial or fungal strains under the tested conditions, as expected, due to sulfonamide resistance. Among the tested compounds, **SA7**, **SA11** and **SA12** showed the highest potency against *S. aureus* strains (*S. aureus* ATCC 43300 (MRSA), *S. aureus* ATCC 25923, *S. aureus* NCTC 6571, and the clinical isolate *S. aureus* 861). Among these three compounds, **SA7** showed the best activity results. Against *S. aureus* ATCC 25923, **SA7** and **SA11** stood out with MIC values of 0.25 and 0.5 μg mL^{-1}, respectively. The activities of **SA7** and **SA12** against MRSA were also noteworthy with MIC values of 1 and 2.5 μg mL^{-1}, respectively.

Moreover, the compounds representing MIC values ≤12.5 μg mL^{-1} on any *S. aureus* strain were selected and tested for their cytotoxic effects against the human fibroblast cell line MRC-5. Additionally, the selectivity index (SI; a ratio that measures the window between cytotoxicity and antimicrobial activity by dividing the given IC_{50} value by the MIC value) was determined for these compounds by selecting the best MICs highlighted in Table 2. Cytotoxicity data as well as the best SI values of the selected SA derivatives are presented in Table 3.

According to the obtained results, the least cytotoxicity was determined for **SA4**, while the most active antibacterial **SA7**, **SA11** and **SA12** derivatives represented IC_{50} values between 30 and 34 μg mL^{-1}. The SI values calculated for these compounds

Table 1 Chemical structures and some properties of the synthesized compounds

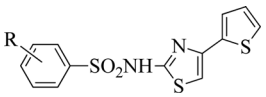

Compound	R	Yield[a] (%)	m.p. (°C)	Molecular weight
SA1	H	70	170–172	322
SA2	4-Br	28	180–182	400
SA3	4-Cl	30	171–173	356
SA4	2,5-diCl	50	132–134	390
SA5	3-NO_2	37	214–216	367
SA6	4-NO_2	51	220–222	367
SA7	4-I	45	199–201	448
SA8	4-CH_3	33	191–193	336
SA9	4-OCH_3	35	182–184	352
SA10	4-$COCH_3$	48	198–200	364
SA11	4-$C(CH_3)_3$	40	212–214	378
SA12	4-C_6H_5	55	200–202	399

[a] Yields of pure isolated products after silica gel column chromatography.

Table 2 Minimal inhibitory concentrations (MICs, μg mL^{-1}) of **SA1–SA12** against the tested *S. aureus* strains

Test organism:	*S. aureus*	MRSA	*S. aureus*	*S. aureus*
Compound	ATCC 25923	ATCC 43300	NCTC 6571	861[a]
SA1	100	50	60	25
SA2	12.5	12.5	25	**6.25**
SA3	12.5	25	25	**6.25**
SA4	12.5	25	25	**6.25**
SA5	50	100	100	50
SA6	100	100	50	25
SA7	**0.25**	1	12.5	0.5
SA8	**12.5**	50	100	25
SA9	25	100	100	50
SA10	100	100	200	50
SA11	**0.5**	6.25	12.5	2.5
SA12	6.25	**2.5**	6.25	**2.5**
ST	>200	>200	>200	150
SD	200	>200	>200	200

[a] Clinical isolate, **ST**-sulfathiazole, **SD**-sulfadiazine.

Table 3 Cytotoxicity of the **SA** derivatives showing anti-*S. aureus* activity against the human fibroblast cell line MRC-5 and the selectivity index values

	SA2	SA3	SA4	SA7	SA8	SA11	SA12
IC_{50} (μg mL^{-1})	37	28	24	30	42	32	34
SI[a]	5.9	4.5	3.8	120	3.4	64	5.4

[a] SI values in comparison to the best MIC values.

ranged from 3.4 to 120. It is worth mentioning that **SA7** and **SA11** exhibited the best SI values of 120 and 64, respectively, on *S. aureus* ATCC 25923. Besides, **SA12** displayed a SI value of 5.4 against MRSA.

Staphylococcus aureus is a Gram-positive bacterium that causes a wide spectrum of conditions ranging from mild skin diseases to severe pneumonia and bacteremia. *S. aureus* resistance to antibiotics has been identified and is associated with extensive mortality.[21] A large proportion of *S. aureus* isolates are resistant to methicillin which is a semi-synthetic penicillin derivative of β-lactam antibiotics. Methicillin-resistant *Staphylococcus aureus* (MRSA) has also been reported to develop resistance to non-β lactam antibiotics such as vancomycin and linezolid.[22,23] Considering the increased rate of death and the burden on the health-care system due to *S. aureus* strains, it is critical to identify novel drug candidates that are selectively effective against this bacterium.

Additionally, the cytotoxic effects of the newly synthesized compounds on healthy cells can be a severe problem throughout the discovery of novel antibacterial agents. Hence, it is of the utmost importance that we identified new sulfonamides with high selectivity indices in the present study.

By analyzing the results according to the chemical structures of the compounds, it is obvious that introducing a thiophene ring into the structure of sulfathiazole made a positive contribution to the antibacterial activities of all derivatives. Additionally, it is worth emphasizing that the most active compounds (**SA7**, **SA11** and **SA12**) carry highly lipophilic substituents at the *para* position of the phenyl ring. The theoretical octanol–water partition coefficients (log *P*) were calculated using Molinspiration[24] for these three derivatives. The log *P* values were found to be 4.30, 4.92 and 5.10 for **SA7**, **SA11** and **SA12**, respectively, and significantly increased compared to the value of 3.21 for **SA1**, a non-substituted phenyl derivative. It is apparent that introducing an aromatic ring (phenyl), a bulky alkyl group (*tert*-butyl) or a voluminous halogen atom (iodine)[25] on the phenyl ring increases the lipophilicity, thus enhancing the antibacterial activity of sulfonamides. Therefore, we conclude that the capability of sulfonamides to penetrate the bacterial membranes of *S. aureus* strains due to increased lipophilicity is one of the factors playing a role in their activities.

Our data showed that **SA7**, **SA11** and **SA12** can kill the pathogenic microorganisms in low amounts without any negative effect on cells, which made them favorable compounds for further experiments.

Methicillin-resistant *Staphylococcus aureus* (MRSA) membrane potential perturbation. MRSA represents a global health problem as a leading cause of mortality from antibiotic-resistant infections. Therefore, new strategies targeting MRSA are of the utmost importance to avert the emerging resistance.[26] As the bacterial membrane plays a significant role in bacterial survival, it stands out as an attractive target for antibacterial agents.[27] Therefore, we measured the potency of our active compounds to disrupt MRSA bacterial membrane potential perturbation, which is considered a membrane-targeting antibacterial activity mechanism. According to the obtained data, **SA7**, **SA11** and **SA12** did not effectively perturb the plasma membrane integrity, contrary to carbonyl cyanide *m*-chlorophenylhydrazone (CCCP), which was used as a positive control (Fig. 5).

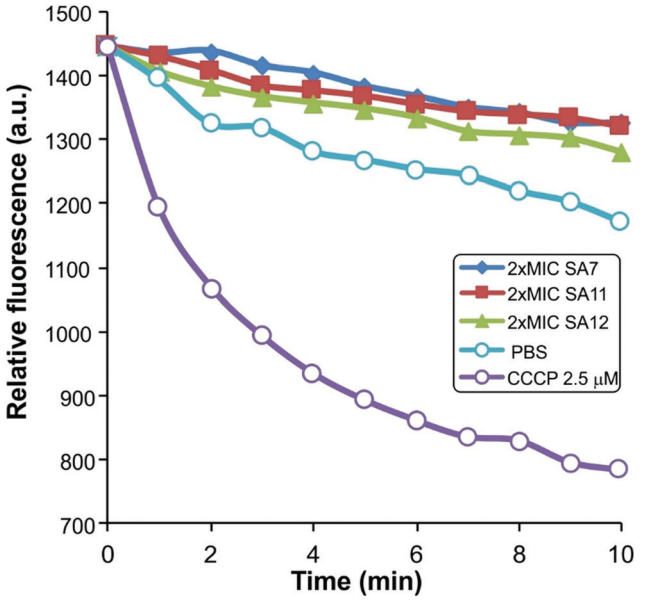

Fig. 5 MRSA membrane potential perturbation upon exposure to **SA7**, **SA11**, and **SA12** (2× MIC values) in comparison to PBS treatment. Sample fluorescence refers to that of the 3,3′-diethyloxacarbocyanine iodide ($DiOC_2(3)$) dye and relates to the membrane potential as previously shown.[28] CCCP (carbonyl cyanide 3-chlorophenylhydrazone) was used as a positive control.

DNA interactions by gel electrophoresis. In many research studies, sulfonamides and their metal complexes are reported to bind DNA.[29–31] Prompted by this information, we also investigated DNA interactions of the most active sulfonamide derivatives (**SA7**, **SA11** and **SA12**). However, the tested compounds did not show any interaction with double-stranded DNA which indicates, at least for these three compounds, that bacterial DNA is not the target for their mode of activity (Fig. S1, ESI†). In general, metal complexes of sulfonamides are reported to bind to DNA with stronger interactions than the ligands.[32] Therefore, we surmise that not testing our compounds as metal complexes can be the determining factor for the lacking interaction with DNA.

Molecular modeling studies

Molecular docking. In order to develop binding hypotheses of the three most active compounds, **SA7**, **SA11** and **SA12**, we performed molecular docking of the compounds into a model of the PABA active site of *S. aureus* strain ATCC 25923 DHPS. The model was based on the X-ray crystal structure of *S. aureus* F17L/E208K double mutant DHPS in the ligand-bound conformation (PDB ID: 6CLV) (Fig. 6A).[33] L17 was restored to F17 using

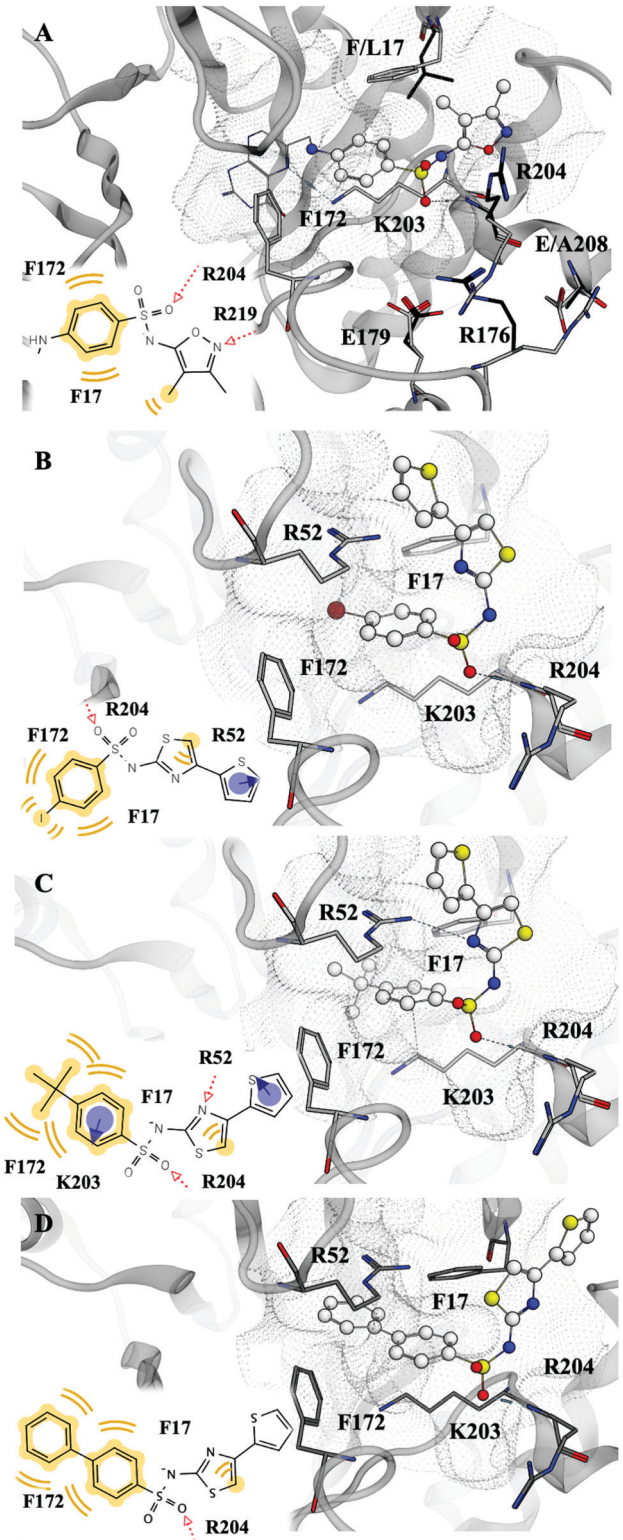

Fig. 6 The *S. aureus* DHPS active site of strain ATCC 25923, featuring the X-ray crystal structure of compound 1530, and the putative docking poses of **SA7**, **SA11** and **SA12**, along with their pharmacophores. (A) The *S. aureus* active site, featuring compound 1530 shown in white (PDB ID: 6CLV). The sulfisoxazole moiety occupying the PABA active site is shown in ball and stick representation, and the pterin moiety occupying the DHPP active site is shown as lines. The pharmacophore of the sulfa moiety of compound 1530 is shown. The E208K mutation causes a rearrangement of the R176-E179-R204-E208 salt bridge. The protein backbone and wildtype residues are shown in grey. The DHPS F17L/E208K double mutant residues are shown in black. K208 is not resolved in the X-ray crystal structure and is shown as A208. (B) The binding hypothesis for **SA7** along with its pharmacophore. (C) The binding hypothesis for **SA11** along with its pharmacophore. (D) The binding hypothesis for **SA12** along with its pharmacophore. Yellow = hydrophobic contact. Red = hydrogen bond acceptor. Mauve = aromatic interaction.

MOE protein builder (v2019.0102)[34] (Fig. 6A and 6B), although the rotamer of F17 in the substrate-bound form of *S. aureus* DHPS described by Griffith *et al.* was not reproducible.[33] This may be because the model generated by Griffith *et al.* was based on an X-ray crystal structure of the DHPS wildtype binding site in *Yersinia pestis* (PDB ID: 3TYZ),[35] which features a different backbone geometry in the loop harboring F17. K208 was restored to E208 and the R176-E179-R204-E208 four-residue salt bridge complex was modelled on X-ray coordinates of wildtype *S. aureus* DHPS (PDB ID: 1AD1)[35] (Fig. 6A). The F17L/E208K double mutant X-ray crystal structure of DHPS from *S. aureus* (PDB ID: 6CLV) features a pterin–sulfonamide hybrid compound including a sulfisoxazole moiety (compound 1530) as a co-crystallized ligand, of which the sulfisoxazole part displaces the natural PABA substrate according to the classic sulfonamide mechanism of action[9,10] (Fig. 6A). Fig. 6B–D depict the binding pose hypotheses of **SA7**, **SA11** and **SA12**, respectively, along with their static pharmacophores. The suggested binding poses were derived from molecular docking and filtered by 3D pharmacophore screening[33] based on the 3D interactions of the bound sulfisoxazole[33] (Fig. 6A), according to the workflow detailed in the Methods section. The poses suggest that the compounds demonstrate a common binding mode, with the phenyl groups occupying the hydrophobic pocket of K203, F17, and F172, which is also occupied by the phenyl group of the natural PABA substrate.[9,33] The phenyl group of **SA11** engages in a further pi-cation interaction with K203. A sulfonyl oxygen of each compound forms a hydrogen bond with the backbone nitrogen of R204. For all three compounds, the substituents on the phenyl ring (iodine, *tert*-butyl and phenyl for **SA7**, **SA11 and SA12**, respectively) point towards the pterin sub-pocket, forming hydrophobic contacts to F17 and F172. The thiazole and thiophene rings of the three compounds extend out of the natural substrate envelope. Each thiazole ring engages in a lipophilic contact with F17, and the thiazole nitrogen of **SA11** engages in a hydrogen bond with R52. The **SA7** and **SA11** thiophene rings engage in a further pi-cation interaction with R52. The thiazole and thiophene rings of **SA12** are rotated 180° about the bond between the sulfonamide nitrogen and the carbon at position 2 of the thiazole ring compared to those of **SA7** and **SA11**, thus adopting the opposite orientation.

Molecular dynamics simulations and dynamic 3D pharmacophores (dynophores). In order to investigate the conformational dynamics of **SA7**, **SA11** and **SA12** within the *S. aureus* ATCC 25923 DHPS binding site, we performed all-atom molecular dynamics (MD) simulations starting from the hypothesized binding pose for each ligand (Fig. 6). As a measure of ligand mobility, we calculated the Root Mean Square Deviation (RMSD) of the ligand heavy atoms (Fig. 7A–C). The RMSD describes the deviation of the atoms from the initial suggested binding pose over the course of the simulation. **SA11** and **SA12** show a higher degree of fluctuation of ligand from the putative pose within the binding site than **SA7** (Fig. 7A–C). To elucidate the molecular basis underlying the mobility of the binding hypotheses within the DHPS active site, dynamic 3D pharmacophores (dynophores) were generated. The dynophore method tracks the ligand–protein interaction pattern over the course of MD simulations, delivering a visual representation of the statistical occurrence of each 3D pharmacophore feature as point density clouds (Fig. 7C–E).[35]

Interestingly, the dynophores uncovered interaction features not seen in the static 3D pharmacophores of the three compounds. In all three molecules, the sulfonamide nitrogen and second sulfonyl oxygen act as hydrogen bond acceptors and the sulfonamide moiety forms a negative ionizable feature (circled in blue in Fig. 7C–E; Table S2, ESI†). Furthermore, for **SA12**, the phenyl rings engage in aromatic interactions, the thiophene ring forms a hydrophobic contact and its thiazole nitrogen forms a hydrogen bond (Fig. 7F and Table S2, ESI†). The **SA11** thiophene ring forms an additional hydrophobic contact as well as aromatic interaction (Fig. 7E and Table S2, ESI†). The **SA7** iodine R-substituent forms a halogen bond, the thiazole ring forms an aromatic interaction, the thiazole nitrogen engages in a hydrogen bond, and the thiophene ring forms an additional hydrophobic contact (Fig. 7D and Table S2, ESI†).

SA11 shows the highest degree of fluctuation of ligand from the putative pose within the binding site, followed by **SA12**, with **SA7** showing the least amount of movement within the DHPS active site (Fig. 7). The dynophores highlight the differences in ligand–enzyme interaction patterns that may explain the increased tendency of **SA11** and **SA12** to deviate from their putative binding poses compared to **SA7**. The iodine as the *R*-substituent of **SA7** forms hydrophobic contacts to PABA active site residues 100% of the time, whereas the **SA11** *tert*-butyl as the *R*-substituent only forms hydrophobic contacts 83% of the time. The **SA7** phenyl group engages in hydrophobic contacts with PABA active site residues for 83% of the simulation trajectory, whereas the **SA11** phenyl group only forms these contacts 63% of the simulation time (Table S2, ESI†). Whereas the sulfonyl oxygens of **SA7** act as hydrogen bond acceptors 42% and 46% of the trajectory, the **SA11** sulfonyl oxygens form hydrogen bonds 27% and 26% of the simulation time (Table S2, ESI†).

The occurrence of the R-substituent hydrophobic interaction is less frequent in **SA12** than in **SA7** (83 *vs.* 100%, respectively). The aromatic interaction of the phenyl group occurs 6% of the time in **SA7** and 1% of the time in **SA12**, and the hydrogen bond to one sulfonyl oxygen occurs over 46% of the **SA7** trajectory and 2% of the **SA12** trajectory. Occurrence frequencies of 1% and 2% are almost negligible.

The dynophore clouds of **SA11** and **SA12** extend into areas of the enzyme not seen in the **SA7** dynophore (labelled as pockets 1–3 in Fig. 7D and F) as **SA11** and **SA12** deviate from their original suggested binding poses to a greater extent, forming more interactions with residues further outside the PABA active site. The occupancy of pocket 3 by the **SA12** thiophene ring is most likely due to the difference in the orientation of this moiety in the putative **SA12** binding pose. We further used these dynophores to explain the activity of the three compounds at *S. aureus* strain ATCC 25923.

Mechanism of activity against *S. aureus* ATCC 25923. SA7 shows the highest activity at *S. aureus* ATCC 25923, followed by **SA11** and then **SA12** (Table 2). The hydrogen bond formed by a sulfonyl oxygen for 46% of the **SA7** trajectory occurs 26% of the

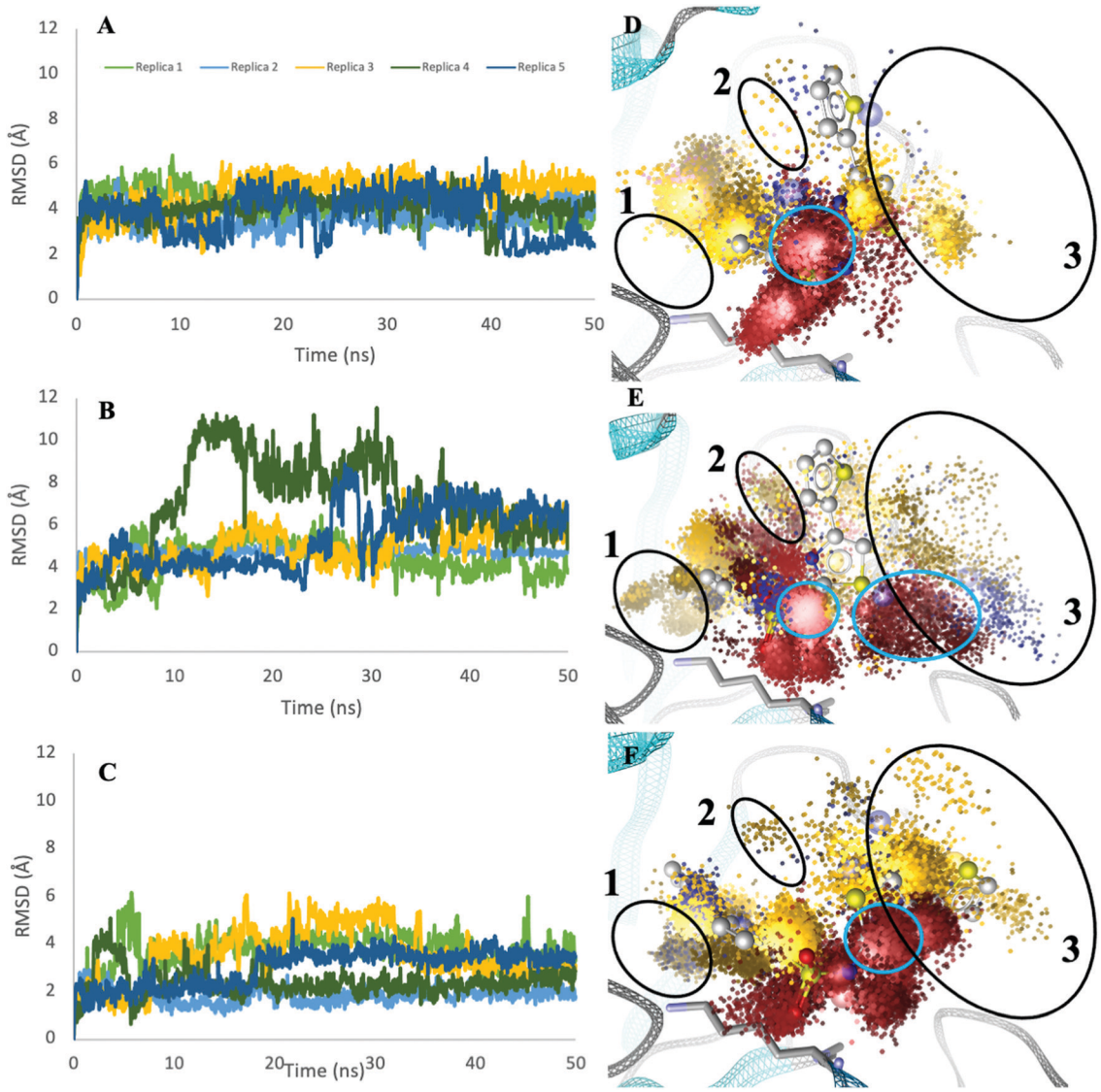

Fig. 7 Investigations into the **SA7**, **SA11** and **SA12** binding hypotheses at the *S. aureus* ATCC 25923 DHPS active site *via* molecular dynamics simulations and dynamic 3D pharmacophores (dynophores). RMSD values of **SA7** (A), **SA11** (B), and **SA12** (C) over the course of five replicates of molecular dynamics simulations. Dynophores of the **SA7** (D), **SA11** (E), and **SA12** (F) binding hypothesis. Pockets into which the **SA7**, **SA11** and **SA12** dynophores spread are circled in black and labelled with the pocket name. Pocket 1 is defined by residues I9, M128, F172 and A199. Pocket 2 is defined by F17, S50, T51 and R52. Pocket 3 is defined by N11, T13, F17, R204, T215, P216 and R219. Negative ionizable feature clouds are circled in blue. Yellow cloud = hydrophobic contact. Blue cloud = aromatic interaction. Red cloud = Hydrogen bond acceptor or negative ionizable feature.

SA11 simulation time, and 2% of the **SA12** trajectory, which is almost negligible. As the occurrence frequency of this hydrogen bond decreases with decreasing compound activity at *S. aureus* ATCC 25923, it could be an underlying cause of this activity trend. Furthermore, the initial binding hypotheses show the **SA12** thiazole and thiophene moieties oriented oppositely to those of **SA7** and **SA11**, and **SA12** displays the fewest number of static modeled interactions. Dynophore analysis shows that **SA12** is able to recapitulate neither the aromatic interaction of the thiazole ring displayed by **SA7** and **SA11** nor the aromatic interaction formed by the **SA-11** thiophene moiety. The **SA12** thiophene also displays the lowest hydrophobic contact occurrence frequency (Table S2, ESI†). This difference in putative binding poses and the resulting dynophore interaction patterns could also contribute to the decreased activity of **SA12** at *S. aureus* ATCC 25923 compared to the other two compounds. Additionally, the reduced potency of **SA11** and **SA12** compared to **SA7** (Table 2) could be explained by the fact that **SA11** and **SA12** are not able to maintain the rigidity of the binding pose within the PABA active site associated with the higher activity of **SA7**.

Experimental

Chemistry

Materials and methods. All reagents were purchased from commercial sources and used as received. Melting points were determined using open glass capillaries and the results are

uncorrected. Infrared (IR) spectra were obtained in the range of 4000–600 cm^{-1} *via* ATR diamond. ^{1}H-(400 MHz) and ^{13}C-NMR spectra (100 MHz) were recorded using a Bruker AM 400 spectrometer in DMSO-d_6 solution. Coupling constants, *J*, are reported in hertz. MS spectra were measured on an Agilent 1200/6530 LC/MS High-Resolution Time of Flight (TOF) instrument at the Atatürk University-East Anatolian High Technology Research and Application Center (DAYTAM).

Synthesis of 2-(bromoacetyl)thiophene (II). Following the method reported in the literature,[37] a solution of bromine (0.81 mL, 15.85 mmol) in CH_2Cl_2 (5 mL) was added dropwise to a solution of 2-acetylthiophene (15.85 mmol) in CH_2Cl_2 (5 mL) at 0 °C. The reaction mixture was stirred at room temperature for 2 h, neutralized with a saturated solution of sodium hydrogen carbonate and extracted with CH_2Cl_2 (3 × 25 mL). The combined CH_2Cl_2 layers were then dried over anhydrous $MgSO_4$ and removed under reduced pressure. A pale yellow oil product was used for the next step without purification.

Synthesis of 4-(thiophen-2-yl)thiazol-2-amine (III). Following the method reported in the literature,[38,39] a solution of 2-bromoacetylthiophene (5.13 g, 0.025 mol) and thiourea (0.03 mol) in ethanol (20 mL) were stirred for 15 min then refluxed for 2 h. Upon cooling, the reaction mixture was made alkaline using 10% sodium hydroxide solution with stirring. The precipitate was collected, washed with water and dried. Recrystallization with ethanol afforded the desired compound. Mp 124–126 °C; ^{1}H NMR (400 MHz, DMSO-d_6) δ 7.37 (dd, J = 8.0, 4.2 Hz, 1H), 7.17 (s, 2H), 7.13–6.95 (m, 1H), 6.83 (s, 1H). ^{13}C NMR (100 MHz, DMSO) δ 168.72, 144.90, 139.62, 128.19, 125.14, 123.19, 100.22. HRMS (EI): $[M + H]^+$, found 183.00452. $C_7H_6N_2S_2$ requires 183.00694.

General procedure for the synthesis of sulfonamides SA1–SA12. A solution of 4-(thiophen-2-yl)thiazol-2-amine 0.15 g (0.81 mmol) and benzenesulfonyl chloride derivatives (1.2 mmol) in dichloromethane and pyridine (15 mL, 12 : 3) were stirred at −5 °C for three days (completion of the reaction was monitored by TLC). After the reaction was completed, the solvent was evaporated in vacuum. The solid residue was purified by column chromatography. Suitable solvent washing and crystallization methods were preferred to obtain the pure product.

***N*-(4-(Thiophen-2-yl)thiazol-2-yl)benzenesulfonamide (SA1).** White solid, R_f (40 : 60 EtOAc : hexane): 0.22; IR (ATR) 3157, 3087, 1517, 1147. ^{1}H NMR (400 MHz, DMSO-d_6) δ 13.34 (bs, 1H, –NH), 7.84 (d, J = 7.6 Hz, 2H), 7.71–7.50 (m, 4H), 7.49 (d, J = 3.7 Hz, 1H), 7.13–7.07 (m, 1H), 7.02 (bs, 1H). ^{13}C NMR (100 MHz, DMSO-d_6) δ 148.40, 146.68, 142.40, 129.54, 129.07, 128.19, 128.13, 127.72, 126.31, 125.93, 103.27. HRMS (EI): $[M + H]^+$, found 322.9978. $C_{13}H_{10}N_2O_2S_3$ requires 322.9983.

4-Bromo-*N*-(4-(thiophen-2-yl)thiazol-2-yl)benzenesulfonamide (SA2). White solid, R_f (40 : 60 : 1 EtOAc : hexane : MeOH): 0.37; IR (ATR) 3246, 3105, 1527, 1134. ^{1}H NMR (400 MHz, DMSO-d_6) δ 13.38 (bs, 1H, –NH), 7.77 (s, 4H), 7.61 (d, J = 5.2 Hz, 1H), 7.49 (d, J = 3.8 Hz, 1H), 7.15–7.08 (m, 1H), 7.03 (s, 1H). ^{13}C NMR (100 MHz, DMSO-d_6) δ 169.03, 141.70, 132.59, 131.76, 128.56, 128.37, 127.83, 126.51, 126.44, 123.22, 103.28. HRMS (EI): $[M + H]^+$, found 400.9081. $C_{13}H_9BrN_2O_2S_3$ requires 400.9088.

4-Chloro-*N*-(4-(thiophen-2-yl)thiazol-2-yl)benzenesulfonamide (SA3). Yellow solid, R_f (40 : 60 EtOAc : hexane): 0.36; IR (ATR) 3246, 3174, 1523, 1180. ^{1}H NMR (400 MHz, DMSO-d_6) δ 13.46 (bs, 1H, –NH), 7.84 (bs, 2H), 7.64 (bd, J = 7.9 Hz, 3H), 7.50 (bs, 1H), 7.12 (d, J = 4.3 Hz, 1H), 7.05 (s, 1H). ^{13}C NMR (100 MHz, DMSO-d_6) δ 168.97, 141.23, 137.55, 131.70, 129.69, 128.60, 128.27, 128.18, 127.89, 126.51, 103.29. HRMS (EI): $[M + H]^+$, found 356.9571. $C_{13}H_9ClN_2O2S_3$ requires 356.9593.

2,5-Dichloro-*N*-(4-(thiophen-2-yl)thiazol-2-yl)benzenesulfonamide (SA4). Pink solid, R_f (50 : 50 : 1 EtOAc : hexane : MeOH): 0.30; IR (ATR) 3174, 3105, 1527, 1134. ^{1}H NMR (400 MHz, DMSO-d_6) δ 13.61 (bs, 1H, –NH), 8.04 (d, J = 2.4 Hz, 1H), 7.76–7.66 (m, 2H), 7.64 (d, J = 5.1 Hz, 1H), 7.54 (d, J = 3.9 Hz, 1H), 7.15–7.11 (m, 1H), 7.06 (s, 1H). ^{13}C NMR (100 MHz, DMSO-d_6) δ 169.69, 141.12, 134.00, 133.77, 132.27, 131.84, 131.47, 130.34, 129.55, 128.58, 127.96, 126.69, 103.71. HRMS (EI): $[M + H]^+$, found 390.9178. $C_{13}H_8Cl_2N_2O_2S_3$ requires 390.9203.

3-Nitro-*N*-(4-(thiophen-2-yl)thiazol-2-yl)benzenesulfonamide (SA5). Yellow solid, R_f (50 : 50 : 1 EtOAc : hexane : MeOH): 0.35; IR (ATR) 3211, 3105, 1537, 1137. ^{1}H NMR (400 MHz, DMSO-d_6) δ 13.60 (bs, 1H, –NH), 8.51 (s, 1H), 8.44 (d, J = 8.5 Hz, 1H), 8.26 (d, J = 8.0 Hz, 1H), 7.87 (t, J = 8.2 Hz, 1H), 7.61 (d, J = 5.1 Hz, 1H), 7.50 (d, J = 3.8 Hz, 1H), 7.15–7.09 (m, 1H), 7.05 (s, 1H). ^{13}C NMR (100 MHz, DMSO-d_6) δ 169.47, 148.20, 144.17, 132.54, 132.32, 131.77, 131.67, 128.56, 127.88, 127.27, 126.54, 120.87, 103.53. HRMS (EI): $[M + H]^+$, found 367.9812. $C_{13}H_9N_3O_4S_3$ requires 367.9833.

4-Nitro-*N*-(4-(thiophen-2-yl)thiazol-2-yl)benzenesulfonamide (SA6). Yellow solid, R_f (60 : 40 : 1 EtOAc : hexane : MeOH): 0.32; IR (ATR) 3263, 3122, 1517, 1137. ^{1}H NMR (400 MHz, DMSO-d_6) δ 13.46 (bs, 1H, –NH), 8.37 (d, J = 8.3 Hz, 2H), 8.08 (d, J = 8.3 Hz, 2H), 7.62 (d, J = 5.0 Hz, 1H), 7.50 (d, J = 3.8 Hz, 1H), 7.12 (d, J = 4.8 Hz, 1H), 7.06 (d, J = 2.7 Hz, 1H). ^{13}C NMR (100 MHz, DMSO-d_6) δ 169.69, 149.81, 147.99, 128.59, 127.92, 127.81, 126.51, 124.97, 124.89, 103.50. (One signal was overlapped). HRMS (EI): $[M + H]^+$, found 367.9807. $C_{13}H_9N_3O_4S_3$ requires 367.9833.

4-Iodo-*N*-(4-(thiophen-2-yl)thiazol-2-yl)benzenesulfonamide (SA7). White solid, R_f (60 : 40 : 1 EtOAc : hexane : MeOH): 0.26; IR (ATR) 3193, 3070, 1531, 1134. ^{1}H NMR (400 MHz, DMSO-d_6) δ 13.34 (bs, 1H, –NH), 7.93 (d, J = 8.3 Hz, 2H), 7.60 (d, J = 7.9 Hz, 3H), 7.55–7.45 (m, 1H), 7.13–7.05 (m, 1H), 7.01 (bs, 1H). ^{13}C NMR (100 MHz, DMSO-d_6) δ 168.91, 142.10, 138.38, 132.35, 131.95, 128.54, 128.10, 127.75, 126.41, 103.24, 100.48. HRMS (EI): $[M + H]^+$, found 448.8930. $C_{13}H_9IN_2O_2S_3$ requires 448.8949.

4-Methyl-*N*-(4-(thiophen-2-yl)thiazol-2-yl)benzenesulfonamide (SA8). Grey solid, R_f (50 : 50 : 1 EtOAc : hexane : MeOH): 0.43; IR (ATR) 3166, 3087, 1527, 1137. ^{1}H NMR (400 MHz, DMSO-d_6) δ 13.22 (s, 1H), 7.74 (d, J = 7.9 Hz, 2H), 7.60 (d, J = 5.1 Hz, 1H), 7.49 (d, J = 3.7 Hz, 1H), 7.36 (d, J = 7.7 Hz, 2H), 7.11 (t, J = 4.5 Hz, 1H), 7.01 (s, 1H), 2.36 (s, 3H). ^{13}C NMR (100 MHz, DMSO-d_6) δ 168.25, 143.03, 139.47, 132.88, 132.21, 129.91, 128.53, 127.61, 126.45, 126.27, 103.12, 21.41. HRMS (EI): $[M + H]^+$, found 337.0118. $C_{14}H_{12}N_2O_2S_3$ requires 337.0139.

4-Methoxy-*N*-(4-(thiophen-2-yl)thiazol-2-yl)benzenesulfonamide (SA9). White solid, R_f (40 : 60 EtOAc : hexane): 0.35; IR (ATR) 3174, 3018, 1537, 1124. ^{1}H NMR (400 MHz, DMSO-d_6) δ 13.23

(bs, 1H, –NH), 7.77 (d, J = 8.5 Hz, 2H), 7.60 (d, J = 5.1 Hz, 1H), 7.48 (d, J = 3.8 Hz, 1H), 7.16–6.87 (m, 4H), 3.80 (s, 3H). ^{13}C NMR (100 MHz, DMSO-d_6) δ 172.56, 162.61, 134.04, 131.88, 128.71, 128.57, 127.64, 126.24, 114.71, 114.65, 103.21, 56.05. HRMS (EI): $[M + H]^+$, found 353.0067. $C_{14}H_{12}N_2O_3S_3$ requires 353.0088.

4-Acetyl-*N*-(4-(thiophen-2-yl)thiazol-2-yl)benzenesulfonamide (SA10). Yellow solid, R_f (50 : 50 : 1 EtOAc : hexane : MeOH): 0.28; IR (ATR) 3246, 3105, 1537, 1134. ^{1}H NMR (400 MHz, DMSO-d_6) δ 13.41 (bs, 1H, –NH), 8.11 (d, J = 8.3 Hz, 2H), 7.97 (d, J = 8.1 Hz, 2H), 7.61 (d, J = 5.1 Hz, 1H), 7.50 (d, J = 3.8 Hz, 1H), 7.11 (t, J = 4.4 Hz, 1H), 7.04 (s, 1H), 2.61 (s, 3H). ^{13}C NMR (100 MHz, DMSO-d_6) δ 197.76, 169.06, 146.06, 139.75, 132.44, 131.81, 129.37, 128.56, 127.83, 126.65, 126.49, 103.34, 27.43. HRMS (EI): $[M + H]^+$, found 365.0058. $C_{15}H_{12}N_2O_3S_3$ requires 365.0088.

4-(*Tert*-butyl)-*N*-(4-(thiophen-2-yl)thiazol-2-yl)benzenesulfonamide (SA11). White solid, R_f (60 : 40 : 1 EtOAc : hexane : MeOH): 0.25; IR (ATR) 3263, 3122, 1537, 1141. ^{1}H NMR (400 MHz, DMSO-d_6) δ 13.07 (bs, 1H, –NH), 7.77 (d, J = 8.0 Hz, 2H), 7.58 (t, J = 8.0 Hz, 3H), 7.48 (d, J = 3.8 Hz, 1H), 7.14–7.06 (m, 1H), 7.02 (d, J = 9.4 Hz, 1H), 1.27 (s, 9H). ^{13}C NMR (100 MHz, DMSO-d_6) δ 168.48, 155.81, 139.50, 132.70, 132.14, 128.56, 127.70, 127.01, 126.34, 126.27, 103.20, 35.26, 31.25. HRMS (EI): $[M + H]^+$, found 379.0593. $C_{16}H_{17}N_2O_2S_3$ requires 379.0609.

***N*-(4-(Thiophen-2-yl)thiazol-2-yl)-[1,1′-biphenyl]-4-sulfonamide (SA12).** White solid, R_f (60 : 40 : 1 EtOAc : hexane : MeOH): 0.25; IR (ATR) 3263, 3122, 1537, 1180. ^{1}H NMR (400 MHz, DMSO-d_6) δ 13.36 (bs, 1H, –NH), 7.93 (m, 7.96–7.89, 2H), 7.90–7.80 (m, 2H), 7.73 (t, J = 6.3 Hz, 2H), 7.65–7.57 (m, 1H), 7.56–7.30 (m, 4H), 7.19–6.93 (m, 2H). ^{13}C NMR (100 MHz, DMSO-d_6) δ 168.65, 144.35, 141.14, 139.09, 132.02, 129.55, 128.87, 128.55, 128.55, 127.76, 127.73, 127.49, 127.02, 126.40, 103.24. HRMS (EI): $[M + H]^+$, found 399.0268. $C_{19}H_{14}N_2O_2S_3$ requires 399.0296.

Biological evaluation

Antimicrobial assays. Stock solutions of sulfonamides **SA1–SA12** were prepared in DMSO at a final concentration of 50 mg mL^{-1} and kept at 4 °C before use, no more than two weeks. Minimal inhibitory concentration (MIC) values against *Staphylococcus aureus* ATCC 25923, *Staphylococcus aureus* NCTC 6571, *Staphylococcus aureus* ATCC43300 (MRSA), *Staphylococcus aureus* isolate 861 (veterinary clinical isolate, Vetlab Ltd, Belgrade, Serbia), *Listeria monocytogenes* NCTC 11994, *Pseudomonas aeruginosa* NCTC 10332, *Escherichia coli* ATCC 11775, and *Candida albicans* ATCC 10231 were determined in Luria-Bertani broth (10.0 g L^{-1} tryptone, 10.0 g L^{-1} NaCl, 5.0 g L^{-1} yeast extract, pH 7.2) and RPMI 1640 medium (Gibco) according to the standard broth microdilution assays.[40] The concentration of inoculum was 5 × 10^5 CFU mL^{-1} for bacterial and 1 × 10^6 CFU mL^{-1} for fungal cells and the maximum tested compound concentration was 200 μg mL^{-1}. The MIC values of growth were obtained by measuring the absorbance at 600 nm (OD600) after overnight incubation at 37 °C using a Tecan Infinite 200 Pro multiplate reader (Tecan Group Ltd, Männedorf, Switzerland). DMSO as a vehicle solvent was used as a control.

Antiproliferative activity assay on a human fibroblast cell line. On a human lung fibroblast cell line (MRC-5), an antiproliferative activity assay with 3-(4,5-dimethylthiazol-2-yl)-2,5-diphenyltetrazolium bromide (MTT) was performed using compounds with MICs of up to 50 μg mL^{-1}.[41] Cells were seeded at a concentration of 1 × 10^4 cells per well in RPMI 1640 medium supplemented with 100 μg mL^{-1} streptomycin, 100 U mL^{-1} penicillin, and 10% (v/v) FBS. Cells were grown in an atmosphere of 95% air and 5% CO_2 at 37 °C and their viability was measured after 48 h. The scope of MTT reduction was measured using the Tecan Infinite 200 Pro multiplate reader (Tecan Group Ltd, Männedorf, Switzerland) by measuring the absorbance at 540 nm. The concentrations of compounds which were able to inhibit cell growth by 50% (IC_{50}) are presented as cytotoxicity indicators.

***Staphylococcus aureus* MRSA membrane potential perturbation.** The depolarization of the membrane potential of *S. aureus* MRSA was determined as described previously.[28] *S. aureus* MRSA was grown in LB medium to the OD_{625nm} of 0.3, and after it was washed with PBS (pH 7.4), 1 × 10^8 CFU mL^{-1} were resuspended in PBS containing 1% (w/v) glucose. The resuspended bacterial cells were incubated for 15 min in a 37 °C shaker (180 rpm), followed by incubation with the 3′-diethyloxacarbocyanine iodide ($DiOC_2(3)$) dye (final concentration of 3 μM) for 30 min in a 37 °C shaker (180 rpm). After the second incubation with the dye, bacterial cells were transferred to a 96 well plate (100 μL per well) and treated with different sulfonamide compounds. The compounds were prepared in a microtiter plate at concentrations of 0.5× MIC, 1× MIC, and 2× MIC. As a negative control, PBS with 1% (w/v) glucose was used, and carbonyl cyanide *m*-chlorophenyl hydrazone (CCCP) as a positive control (final concentration of 0.025 μM). Immediately after the addition of compounds, using a Tecan Infinite 200 Pro multiplate reader (Tecan Group Ltd, Mannedorf, Switzerland), the fluorescence change was measured (excitation 485 nm, emission 630 nm).

DNA interactions by gel electrophoresis. The DNA interaction assay was performed using the commercial lambda bacteriophage DNA (300 ng, Thermo Scientific™) according to the previously published procedure.[42] 20 ng μL^{-1} of DNA solution was incubated with 400 μM, 200 μM, and 100 μM of compounds in a 15 μL reaction volume at 37 °C for 1 h. After the period of incubation, the samples were mixed with a loading dye and run on 0.8% (w/v) agarose gel containing ethidium bromide (EtBr) at 60 V for 1 h. HyperLadder™ 1 Kb Plus DNA Ladder (FastGene) was used as standart. Results were obtained using the Gel Doc EZ system (Bio-Rad, Life Sciences, Hercules, USA), equipped with the Image Lab™ software.

Molecular modeling studies

Molecular docking. The X-ray coordinates of double mutant ligand-bound DHPS from *S. aureus* (PDB ID: 6CLV)[33] were taken as the template protein conformation and prepared and restored to wildtype in the MOE protein builder (v2019.0102).[34] The mutant residues F17L and E208K were restored to wildtype and energy-minimized using the OPLS-AA forcefield,[43] and the R176-E179-R204-E208 salt bridge conformation was modelled manually according to the X-ray coordinates of wildtype *S. aureus* DHPS in the apo form (PDB ID: 1AD1). The unresolved 6-residue loop D19-N24 was modelled using the loop modeller function in MOE. The resulting models had no geometric outliers.

The enzyme structures were protonated at pH 7.4 using Protonate3D.[44] The 3D structures of compounds **SA7**, **SA11** and **SA12** were generated using ChemDraw (v18.1; PerkinElmer Informatics) and Corina (v3.0; Molecular Networks GmbH).[45]

Compounds **SA7**, **SA11** and **SA12** were flexibly docked into the rigid modelled wildtype structure of DHPS from *S. aureus* using GOLD (v.5.2; Genetic Optimization for Ligand Docking, The Cambridge Crystallographic Data Centre, UK).[46] The sulfonyl sulphur was used as the center of the binding site sphere and the radius was set to 10 Å. The genetic algorithm (GA) performed 50 runs at 100% efficiency and was set to generate diverse solutions. The resulting 50 binding hypotheses were energy-minimized using the MMFF94 forcefield[47] in LigandScout (v 4.4, Inte:Ligand, Vienna, Austria)[48–50] in the presence of the wildtype *S. aureus* DHPS model.

The poses were filtered according to how well they fulfil the features of the 3D pharmacophore model of the sulfa moiety of the compound co-crystallized in the F17L/E208K DHPS X-ray crystal structure (PDB ID: 6CLV)[33] (Fig. 6A). Compounds in which the phenyl group did not overlap with the phenyl group of the co-crystallized ligand in the hydrophobic pocket of the PABA catalytic site were rejected. Only binding modes wherein a sulfonyl oxygen forms hydrogen bonds with the backbone nitrogen of R204 were retained. Binding hypotheses were further filtered by the number of interactions with the protein and by the fit of the compound into the PABA active site.

Molecular dynamics simulations. The complexes of *S. aureus* in complex with **SA7**, **SA11**, **SA12** and the co-crystallized ligand were prepared in Maestro (v11.7),[51] and 5 replicates of unrestrained molecular dynamics simulation of each system were performed using Desmond (v. 5.5)[52] and the OPLS-AA forcefield.[43] The simulations were performed on water-cooled Nvidia GeForce RTX 2080 Ti graphics cards (NVIDIA corporation, Santa Clara, USA). Systems were solvated in a cubic water box with 15 Å padding to the protein surface using TIP4P water molecules.[53] Sodium ions were added to neutralize the system, and NaCl was added to a physiological concentration of 0.15 M. Simulations were run for 50 ns, and 1000 ligand–complex conformations were obtained for each replicate. Simulations were performed at a constant pressure of 1.01325 bar using the Martyna–Tobias–Klein method and a temperature of 300 K using the Nose–Hoover chain method. Intermolecular forces were calculated using the RESPA integrator with a standard interaction cutoff of 9.0 Å. VMD (v1.9.3)[54] was used for the visual inspection of the conformational trajectory of the ligands and for the calculation of RMSD values.

Dynamic 3D pharmacophores (dynophores). The dynophore approach combines static 3D pharmacophore modelling with conformational sampling of the ligand–enzyme complex through molecular dynamics (MD) simulations.[36] The five MD simulation replicates of each ligand–enzyme system were concatenated and aligned to the heavy atoms of the starting conformation. A 3D pharmacophore model was generated for each enzyme–ligand conformation generated during the MD simulations. Interaction features are categorized as aromatic, hydrophobic, charged interactions, or hydrogen bonds, and are grouped together according to the ligand atoms involved in the feature. The resulting so-called 'superfeatures' are then represented as density clouds (Fig. 7D–F) according to their statistical occurrence throughout the course of the MD simulation and which protein residues are involved. Dynophores offer a deeper analysis of protein–ligand interaction dynamics, for example, to explain the effect of resistance mutations on CYP4Z1 substrate recognition.[55] Dynophores have provided insights into the plasticity of the arginase catalytic site, resulting in the development of two arginase inhibitors, which hold the potential to inform the development of anticancer therapeutics.[56] Dynophores have also been used to explain an activity cliff between two M2 receptor ligands[36] and to uncover a mechanism of bypassing drug resistance in HIV-reverse transcriptase.[57] The dynophore method is fully automated and implemented in the LigandScout framework.[48–50]

Conclusion

The discovery of sulfonamides as the first class of synthetic antibacterial agents initiated the golden era in the management of bacterial infections. With their wide spectrum of antibacterial activities, sulfonamides were successfully used for more than 75 years to control bacterial infections until the development of prevalent drug resistance. In the present work, we aimed to overcome this sulfonamide resistance through rational molecular modifications. Therefore, we synthesized twelve new modified sulfonamide derivatives based on the structure of sulfathiazole, a well-known antibacterial sulfa drug. Introducing a thiophene ring into the main scaffold and lipophilic substituents at the *para* position of the phenyl ring led to a significant increase in the antibacterial activities of the compounds against *S. aureus*. Three compounds (**SA7**, **SA11** and **SA12**) represent the most attractive ones in this series with low MIC values and low cytotoxicity against healthy human lung fibroblasts as well. The MRSA membrane potential perturbation and DNA interaction characteristics of **SA7**, **SA11** and **SA12** indicated that these mechanisms are unlikely to play a role in the antibacterial activity of these compounds. Molecular docking of **SA7**, **SA11** and **SA12** into the *S. aureus* ATCC 25923 DHPS active site shows a commonly hypothesized binding mode for **SA7** and **SA11**, with the thiazole and thiophene rings of **SA12** adopting a different conformation to the former two compounds. Thiophene ring and lipophilic substituents (iodine, *tert*-butyl and phenyl) provided additional aromatic and hydrophobic interactions with DHPS. Molecular dynamics simulations underline that **SA7** is able to retain its original suggested binding pose to a higher degree than **SA11** and **SA12**, in line with its increased potency. This difference in ligand rigidity within the active site could be explained by dynamic 3D pharmacophore analysis, which elucidated the differences in ligand–enzyme interaction patterns between the three compounds. The activity trend followed by the compounds at *S. aureus* ATCC 25923 could be traced back to the occurrence frequency of a hydrogen bond formed by a sulfonyl oxygen. Altogether, these data suggest a new approach to modify sulfa drugs to overcome sulfonamide resistance and improve the antibacterial activity, particularly against *S. aureus* strains.

Conflicts of interest

The authors declare that they have no known competing financial interests or personal relationships that could have appeared to influence the work reported in this paper.

Acknowledgements

Ş. D. D. and Z. K. are grateful to the Research Foundation of Erciyes University (Project Number: FBA-2017-7340) for the financial support of this work. We thank the Sonnenfeld Foundation for the financial support to T. N., S. S. B., S. V. and J. N. R. are partially supported by Ministry of Education, Science and Technological Development of the Republic of Serbia, 451-03-9/2021-14/ 200042.

References

1 N. Zhang and S. Ma, *Eur. J. Med. Chem.*, 2019, **184**, 111743.
2 M. J. Renwick, D. M. Brogan and E. Mossialos, *J. Antibiot.*, 2016, **69**, 73–88.
3 R. Vivas, A. A. T. Barbosa, S. S. Dolabela and S. Jain, *Microb. Drug Resist.*, 2019, **25**, 890–908.
4 F. A. Khan, S. Mushtaq, S. Naz, U. Farooq, A. Zaidi, S. M. Bukhari, A. Rauf and M. S. Mubarak, *Curr. Org. Chem.*, 2018, **22**, 818–830.
5 F. Carta, A. Scozzafava and C. T. Supuran, *Expert Opin. Ther. Pat.*, 2012, **22**, 747–758.
6 S. Apaydın and M. Török, *Bioorg. Med. Chem. Lett.*, 2019, **29**, 2042–2050.
7 T. Nasr, S. Bondock and S. Eid, *Eur. J. Med. Chem.*, 2014, **84**, 491–504.
8 C. Capasso and C. T. Supuran, *Bacterial Resistance to Antibiotics – From Molecules to Man*, Wiley, 2019, pp. 163–172.
9 Y. Zhao, W. R. Shadrick, M. J. Wallace, Y. Wu, E. C. Griffith, J. Qi, M. K. Yun, S. W. White and R. E. Lee, *Bioorg. Med. Chem. Lett.*, 2016, **26**, 3950–3954.
10 M. K. Yun, Y. Wu, Z. Li, Y. Zhao, M. B. Waddell, A. M. Ferreira, R. E. Lee, D. Bashford and S. W. White, *Science*, 2012, **335**, 1110–1114.
11 O. Sköld, *Drug Resist. Updates*, 2000, **3**, 155–160.
12 S. T. Gaballah, H. Amer, A. Hofinger-Horvath, M. Al-Moghazy and M. I. Hemida, *Egypt. J. Chem.*, 2020, **63**, 171–184.
13 L. Lima and E. Barreiro, *Curr. Med. Chem.*, 2012, **12**, 23–49.
14 C. W. Thornber, *Chem. Soc. Rev.*, 1979, **8**, 563–580.
15 E. D. Brown and G. D. Wright, *Nature*, 2016, **529**, 336–343.
16 L. A. Dutra, T. R. F. de Melo, C. M. Chin and J. L. Santos, *Currículo Lattes*, 2012, 001–009.
17 R. F. Battisti, Y. Zhong, L. Fang, S. Gibbs, J. Shen, J. Nadas, G. Zhang and D. Sun, *Mol. Pharm.*, 2007, **4**, 140–153.
18 R. Mishra, I. Tomar, S. Singhal and K. K. Jha, *Der Pharma Chem.*, 2011, **3**, 38–54.
19 R. Mishra, N. Sachan, N. Kumar, I. Mishra and P. Chand, *J. Heterocycl. Chem.*, 2018, **55**, 2019–2034.
20 W. Zhang, Z. Wei, G. Huang, F. Xie, Z. Zheng and S. Li, *Bioorg. Med. Chem.*, 2020, **28**, 115777.
21 T. A. Taylor and C. G. Unakal, *Staphylococcus Aureus*, StatPearls Publishing, Treasure Island (FL), 2019.
22 M. Mizusawa and K. C. Carroll, *Expert Rev. Anti-Infect. Ther.*, 2020, 759–778.
23 P. Dharmaratne, D. N. Sapugahawatte, B. Wang, C. L. Chan, K. M. Lau, C. Lau, K. P. Fung, D. K. Ng and M. Ip, *Eur. J. Med. Chem.*, 2020, **200**, 112341.
24 Molinspiration, https://www.molinspiration.com/cgi-bin/properties.
25 R. Wilcken, M. O. Zimmermann, A. Lange, A. C. Joerger and F. M. Boeckler, *J. Med. Chem.*, 2013, **56**, 1363–1388.
26 A. Antonoplis, X. Zang, M. A. Huttner, K. K. L. Chong, Y. B. Lee, J. Y. Co, M. R. Amieva, K. A. Kline, P. A. Wender and L. Cegelski, *J. Am. Chem. Soc.*, 2018, **140**, 16140–16151.
27 R. M. Epand, C. Walker, R. F. Epand and N. A. Magarvey, *Biochim. Biophys. Acta, Biomembr.*, 2016, **1858**, 980–987.
28 D. L. Higgins, R. Chang, D. V. Debabov, J. Leung, T. Wu, K. M. Krause, E. Sandvik, J. M. Hubbard, K. Kaniga, D. E. Schmidt, Q. Gao, R. T. Cass, D. E. Karr, B. M. Benton and P. P. Humphrey, *Antimicrob. Agents Chemother.*, 2005, **49**, 1127–1134.
29 M. Salehi, M. Kubicki, M. Galini, M. Jafari and R. E. Malekshah, *J. Mol. Struct.*, 2019, **1180**, 595–602.
30 B. Macías, M. V. Villa, B. Gómez, J. Borrás, G. Alzuet, M. González-Álvarez and A. Castiñeiras, *J. Inorg. Biochem.*, 2007, **101**, 444–451.
31 A. Abbas, S. Murtaza, M. N. Tahir, S. Shamim, M. Sirajuddin, U. A. Rana, K. Naseem and H. Rafique, *J. Mol. Struct.*, 2016, **1117**, 269–275.
32 R. B. Dixit, *Sci. Pharm.*, 2011, **79**, 293–308.
33 E. C. Griffith, M. J. Wallace, Y. Wu, G. Kumar, S. Gajewski, P. Jackson, G. A. Phelps, Z. Zheng, C. O. Rock, R. E. Lee and S. W. White, *Front. Microbiol.*, 2018, **9**, 1–16.
34 Chemical Computing Group Inc, 2015, 0.1010. Sherbrooke St. West, Suite #910.
35 I. C. Hampele, A. D'Arcy, G. E. Dale, D. Kostrewa, J. Nielsen, C. Oefner, M. G. P. Page, H. J. Schönfeld, D. Stüber and R. L. Then, *J. Mol. Biol.*, 1997, **268**, 21–30.
36 A. Bock, M. Bermudez, F. Krebs, C. Matera, B. Chirinda, D. Sydow, C. Dallanoce, U. Holzgrabe, M. De Amici, M. J. Lohse, G. Wolber and K. Mohr, *J. Biol. Chem.*, 2016, **291**, 16375–16389.
37 G. Gudipudi, S. R. Sagurthi, S. Perugu, G. Achaiah and G. L. D. Krupadanam, *RSC Adv.*, 2014, **4**, 56489–56501.
38 A. M. Farag, H. M. Hassaneen, I. M. Abbas, A. S. Shawali and M. S. Algharib, *Phosphorous Sulfur Relat. Elem.*, 1988, **40**, 243–249.
39 Ş. D. Doğan, S. Uğır, A. K. K. Arslan, E. Öztürk, A. Cuaoğlu and M. B. Yerer, *Sağlık Bilim. Derg.*, 2019, **28**, 87–93.
40 S. N. Sovari, S. Vojnovic, S. S. Bogojevic, A. Crochet, A. Pavic, J. Nikodinovic-Runic and F. Zobi, *Eur. J. Med. Chem.*, 2020, **205**, 112533.
41 M. B. Hansen, S. E. Nielsen, K. Berg, E. Nielsen and K. Berg, *J. Immunol. Methods*, 1989, **119**, 203–210.
42 N. D. Savić, S. Vojnovic, B. Glišić, A. Crochet, A. Pavic, G. V. Janjić, M. Pekmezović, I. M. Opsenica, K. M. Fromm,

J. Nikodinovic-Runic and M. I. Djuran, *Eur. J. Med. Chem.*, 2018, **156**, 760–773.
43 W. L. Jorgensen, D. S. Maxwell and J. Tirado-Rives, *J. Am. Chem. Soc.*, 1996, **118**, 11225–11236.
44 P. Labute, *Proteins: Struct., Funct., Bioinf.*, 2009, **75**, 187–205.
45 J. Sadowski, J. Gasteiger and G. Klebe, *J. Chem. Inf. Comput. Sci.*, 1994, **34**, 1000–1008.
46 G. Jones, P. Willett, R. C. Glen, A. R. Leach and R. Taylor, *J. Mol. Biol.*, 1997, **267**, 727–748.
47 T. A. Halgren and R. B. Nachbar, *J. Comput. Chem.*, 1996, **17**, 587–615.
48 T. Seidel, G. Ibis, F. Bendix and G. Wolber, *Drug Discovery Today Technol.*, 2010, **7**, e221–e228.
49 G. Wolber and W. Sippl, in *The Practice of Medicinal Chemistry*, 4th edition, ed. C. G. Wermuth and D. Rognan, Elsevier Ltd, Philadelphia, PA, USA, 2015, pp. 489–507.
50 G. Wolber and T. Langer, *J. Chem. Inf. Model.*, 2005, **45**, 160–169.
51 M. S. Ll., Schrödinger Release 2017-2 Maest., 2017.
52 S. Ll., *Schrödinger Release 2015-4: Desmond molecular dynamics system, Maestro-Demond interoperability toops*, DE Shaw Research, 2015.
53 H. W. Horn, W. C. Swope, J. W. Pitera, J. D. Madura, T. J. Dick, G. L. Hura and T. Head-Gordon, *J. Chem. Phys.*, 2004, **120**, 9665–9678.
54 W. Humphrey, A. Dalke and K. Schulten, *J. Mol. Graphics*, 1996, **14**, 33–38.
55 W. Du, D. Machalz, Q. Yan, E. J. Sorensen, G. Wolber and M. Bureik, *Biochem. Pharmacol.*, 2020, **174**, 113850.
56 J. Mortier, J. R. C. Prévost, D. Sydow, S. Teuchert, C. Omieczynski, M. Bermudez, R. Frédérick and G. Wolber, *Sci. Rep.*, 2017, **7**, 1–9.
57 B. Nizami, D. Sydow, G. Wolber and B. Honarparvar, *Mol. BioSyst.*, 2016, **12**, 3385–3395.